Imaging of the ejection process of nanosecond laser-induced forward transfer of gold

R. Pohl[*1], C.W. Visser[*2], G.R.B.E. Römer[*1], C. Sun[*2], A.J. Huis in't Veld[*1] and D. Lohse[*2]

[*1] *Chair of Applied Laser Technology, Faculty of Engineering Technology, University of Twente, The Netherlands*
E-mail: r.pohl@utwente.nl
[*2] *Physics of Fluids, Faculty of Science and Technology, Mesa+ Institute, University of Twente, The Netherlands*

Laser-induced forward transfer is a direct-write process suitable for high precision 3D printing of several materials. However, the driving forces related to the ejection mechanism of the donor material are still under debate. So far, most of the experimental studies of nanosecond LIFT, are based on post process analysis of either the donor layer and/or the deposits, which were transferred to the receiving substrate. To gain further insights into the ejection dynamics, this article presents results of a series of imaging experiments of the release process of nanosecond LIFT of a 200 nm thick gold donor layer. Images were obtained using a setup which consists of two dual-shutter cameras. Both cameras were combined with a 50× long-distance microscope and used to capture coaxial and side-view images of the ejection process. Bright field illumination of the scene was accomplished by a 6 ns dual-cavity laser source. For laser fluence just above the transfer threshold, the formation of a jet and the subsequent release of a single droplet was observed. The droplet diameter was estimated to be about 2 µm. Analysis of the coaxial images indicates the emission of a spectral broad range light which was identified as thermal radiation.

Keywords: Laser-induced forward transfer, high-speed imaging, metal droplets, metal printing

1. Introduction

Laser-induced forward transfer (LIFT) is a 3D direct-write method suitable for precision printing of various materials. The process has been demonstrated first in 1986 by Bohandy et al [1]. The process consists of a ideally completely transparent carrier which is precoated with a thin layer of the material of choice to be transferred, see Fig. 1. The ejection process is initiated by a single laser pulse, with typical pulse durations in the order of nano- to femtoseconds. Depending on the experimental conditions, stress relaxation and/or partial vaporization of the donor layer results in an ejection of the molten donor material and subsequent deposition on a receiving substrate. Size and morphology of the deposits depend on the laser fluence applied, indicating that several physical processes determine the ejection process. Applications of LIFT of thin metal layers can be found in metal filling of 3D-etched Through Silicon Vias (TSVs) and deposition of 2D metal conducting tracks in the semiconductor industry [2]. These applications directly benefit from the advantages of LIFT being a maskless, solvent-free deposition process, which can be performed in ambient atmosphere at room temperature without the use of any (wet) chemicals.

However, the LIFT process still suffers from uncontrolled contamination (deposits) on the receiving substrate. In order to gain further insights and to achieve an in-depth understanding of LIFT, time–resolved images of the ejection have been studied. Unfortunately, time-resolved visualization of the ejection has been achieved only for relatively thick liquid-film [3-5] and solid-phase [6] transfer processes. Other observations of LIFT processes of Au [7], Ni [8] and Cr [9] did not achieve sufficient spatial resolutions to trace the process in detail. However, imaging studies on copper indicate different ejection mechanisms for nanosecond [10] and picosecond LIFT [11] using laser fluences just above the transfer threshold. Recent publications captured the ejection process of femtosecond LIFT of Au [12], using a layer thickness of 60 nm. It was found that, for laser fluence levels just above the transfer threshold, the formation of a liquid jet is caused by the hydrodynamic behavior of the molten donor layer. It has been shown, that for donor layers with an donor layer thickness of 200 nm, the ejection dynamics of picosecond LIFT are significantly different from prior observations, as multiple ejection regimes have been observed [13].

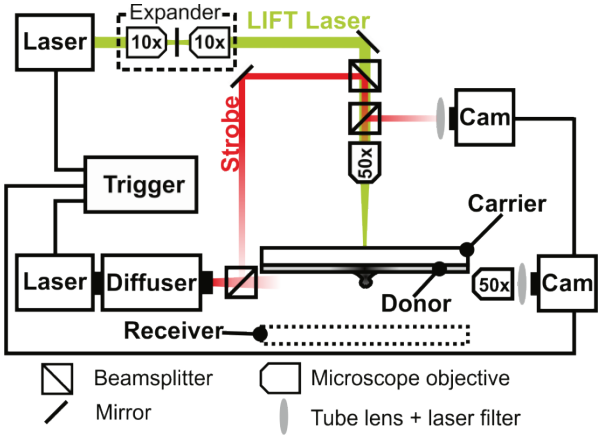

Fig. 1 Sketch of the LIFT and imaging experimental setup.

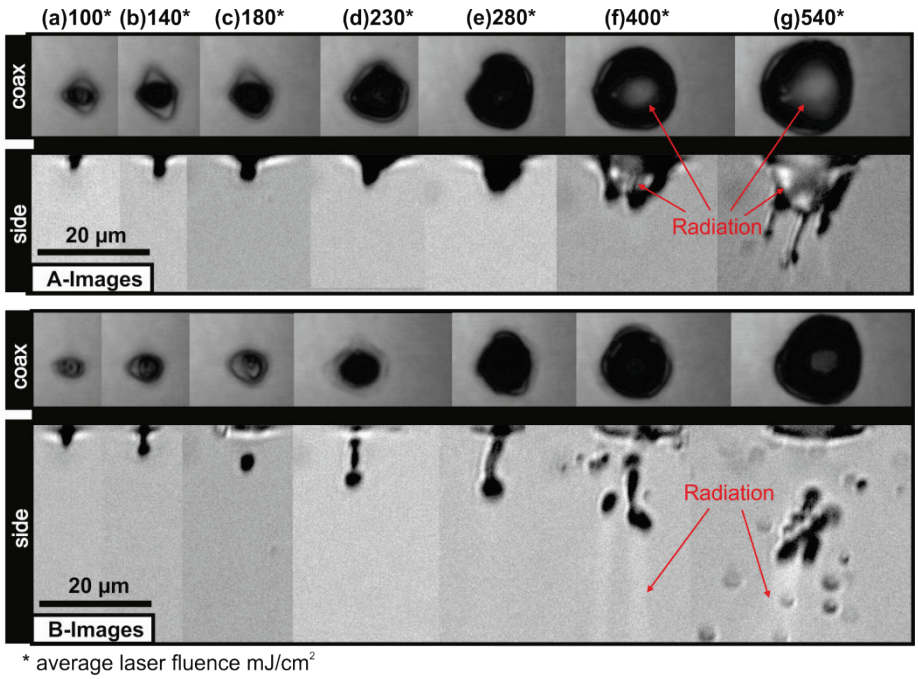

Fig. 2 A and B images of the coaxial and side-view of the nanosecond LIFT ejection process. (b) - (e) Laser fluence levels just above the transfer threshold of 140 mJ/cm^2 lead to the formation of a liquid jet, which subsequently contracts into a droplet. (f) - (g) Increasing laser fluences lead to an uncontrolled ejection process, indicated by the formation of blistering gold bubble.

This article presents further experimental results of LIFT of 200 nm gold using a nanosecond laser source. In section 2, a brief description of the experimental LIFT set-up and imaging setup is presented. In section 3, fluence resolved image sequences composed of side and coaxial views are discussed. In addition, time-resolved images of the low fluence regime and the observation of thermal radiation from the heated droplets are discussed.

2. Experimental methods

Figure 1 shows schematic drawing of the experimental LIFT setup. LIFT experiments were performed using a 6 ns, frequency doubled Nd:YAG laser source emitting at a central wavelength of 532 nm. The laser was focused onto the carrier-donor-interface using a 50x long-working distance objective. The laser spot size (1/e^2) was measured to be 10±1µm. The laser fluence applied during the experiments are expressed in terms of average fluence values [14]. Extra-white soda lime glass was used as a carrier substrate. This carrier was precoated with a 200 nm thick layer of gold, using magnetron sputtering with a sputter rate of 23 nm/m. A beam expander in the LIFT beam path was used to align the focal plane of the LIFT laser beam with the imaging plane of the coaxial imaging setup.

High-resolution images of the LIFT ejection process were captured from two perspectives. First, the side view images were recorded using a combination of a dual shutter camera and a dual cavity nanosecond laser source. The later was used as a stroboscopic light source to illuminate the scene. In order to increase the contrast and to avoid interference effects a fluorescence based high efficiency diffuser was placed in the beam path of the strobe laser. A high spatial resolution was achieved by a combination of an 50x long-working distance objective and a 200 mm tube lens. In order to suppress light from the LIFT laser source entering the camera, a long-pass filter was placed in the infinite pass of the microscope setup. For the second perspective - i.e. the coaxial view of the ejection process - the optical axis of the second dual shutter camera was aligned with the LIFT beam path. The imaging was obtained through the same 50x long working distance objective which was used to focus the LIFT laser beam onto the carrier-donor-interface. Also this objective was combined with a 200 mm infinite corrected tube lens, that was mounted to the camera. Any reflection of the focused LIFT laser beam, was suppressed using a long-pass filter. To achieve a high temporal resolution, the coaxial and the side view cameras share the same strobe source. The timing of the imaging setup with respect to the LIFT laser was achieved using a BNC pulse delay generator. The temporal jitter was estimated to be less than 10 ns. By combining the dual-shot camera with the dual-cavity strobe illumination source, each ejection event was captured twice (referred to in the following as image A and B) with a temporal delay between the images of 500 ns.

3. Results and discussion

3.1 Fluence scan

Figure 2 shows the ejection process obtained at difference laser fluence values. Starting from a fluence level of 100 mJ/cm^2, just below the transfer threshold fluence of 140 mJ/cm^2, the laser fluence was increased up to 540 mJ/cm^2. Each ejection was captured at two time instances (300 ns and 800 ns) after the start of the LIFT laser pulse, indicated by the A- and B-images in Fig. 2. Both top (coaxial) view and side view images of the donor layer are shown. Below the threshold fluence of 140 mJ/cm^2 indicated by figures (a) and (b) no ejection is observed. Instead, a resolidified

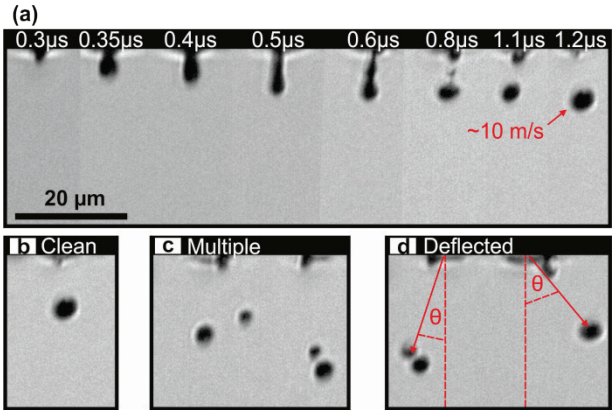

Fig. 3 Ejection process captured at a laser fluence level of 230 mJ/cm^2. (a) Formation and subsequent contraction of a liquid gold jet into (b) a single droplet, (c) multiple droplets (two ejections shown) and (d) a deflected single (right) or multiple droplets (left). The timings are indicated on top.

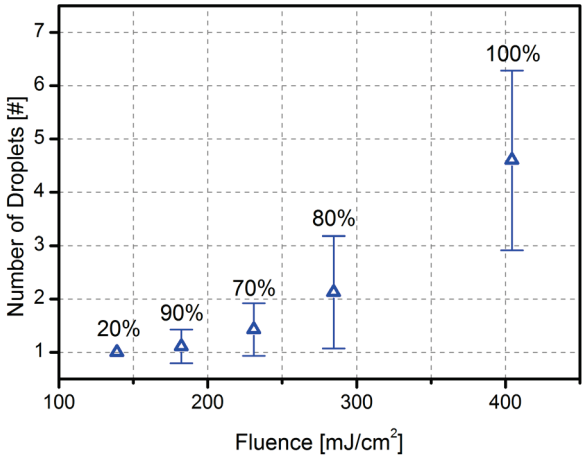

Fig. 4 Observed number of droplets as a function of the laser fluence.

(frozen) jet, i.e. a non-ejection event was captured. Comparing the A- and the B-images shows a solely deformed jet, which is characterized by an partially contracted jet, resulting into the partial formation of a droplet at the tip of the jet. For slightly higher fluence levels, i.e. figures (c) - (e) the formation of an initially arbitrary deformed dome can be identified in the A-image. At a later instance (B-images), this ejected dome contracted into a jet like feature, with an contracted droplet at the tip. At this point the ejection process seems to be dominated by the full melting and the resulting stress relaxation of the heated gold layer, similar to what has been reported for femtosecond LIFT of 60 nm gold layers [11]. Figures (f) – (g) show the ejection process at higher laser fluence levels. For fluence levels above 400 mJ/cm^2 the formation of a strongly deformed bubble is observed, see A-images. The rupture of these bubbles, from the donor layer, lead to an uncontrolled ejection process, which is characterized by an ejection of multiple droplets, as can be observed in the B-images.

In addition to the side view images, the coaxial images are presented. These images indicate the increasing crater diameter towards higher laser fluence values, which is related to the Gaussian beam distribution of the focused LIFT laser beam. Comparing the A- and B-images shows a reflow of material as the crater diameter decreases over time. This unexpected observation maybe explained by the liquid behavior of the molten gold and the relaxation of the prior formed gold bubble resulting in a reflow of material. However, the exact details of the physics involved are yet unknown and is subject of future study.

3.2 Low fluence

Figure 3 shows the ejection process recorded at a laser fluence level of 230 mJ/cm^2. Figure 3 (a) shows a time-resolved image series that was chosen to give an qualitative impression of the ejection process. Beginning at 300 ns after the laser pulse, subsequently, the initially flat donor layer deforms into a liquid jet, which is still connected to the donor layer, i.e. to the melt pool that is generated from the absorbed laser pulse. At 600 ns, the jet reaches a critical length at which the surface tension an instability of the liquid jet. As a result, a droplet is separated from the jet as observed at 800 ns. Here, the ejection speed was measured to be approximately 10 m/s.

Due to the instability, more than one droplet can be observed. The ejections are stochastic in nature. That is, figure (b) shows three typical observations made during the experiments. Obtained at identical experimental conditions, either (i) clean (59%), (ii) multiple (41%) or (iii) deflected ejections of either a single or multiple droplets were observed. In contrast to prior observations, those deflected ejections do not propagate perpendicular to the donor layer, but were deflected at an angle ($0°\leq\theta\leq42.5°$). The cause of this deflection is not understood yet. However, asymmetry of the power density profile of the focused LIFT laser beam and/or irregular thickness of the donor layer may lead to instabilities during the subsequent breakup of the observed jets into droplets.

Figure 4 shows the number of identified droplets as a function of the applied laser fluence. Increasing the laser fluence results in an increase of the averaged observed droplets, as well as an increase in the measured standard deviation. The percentage of distinctive ejection events for each fluence values is added as label to each marker. Due to the lack of sufficient data (20%) at the transfer threshold, the observation at 140 mJ/cm^2 does not show an error bar. However, it is clear that a clean ejection may be expected only for fluence values just above the threshold, as an increased fluence directly increases the number of undesired observed droplets.

3.3 Broad band radiation

Fig. 2 (f) and (g) show broad band radiation (bright areas), observed both in the side view and coaxial view images. In the following, a first interpretation of the origin of the observed radiation is discussed. First of all, it needs to be discussed, whether the observed light is related to the heating of the gold layer or originates from the carrier material (soda-lime glass). Figure 5 shows a series of coaxial images that were obtained after four laser pulses at a fixed laser fluence captured at a fixed time-delay of 10 ns after the LIFT laser pulse. Each image shows the same crater in the donor layer, after each laser pulse. The bright radiation can be clearly observed due to the first and second laser pulse, but not due to the third and fourth. That is, after the

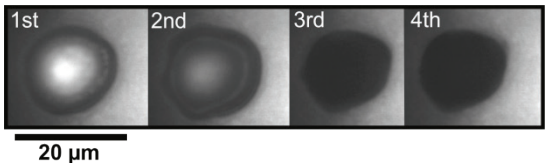

Fig. 5 Coaxial view on the donor layer, which is subsequently exposed to four laser pulses. The bright radiation signal which can be observed at the first and second image disappears completely after the second laser pulse.

second laser pulse only the prior formed crater in the donor layer is visible. As the detected radiation signal is not persistent over multiple laser pulses, it is concluded that the source of radiation cannot originate from the carrier material, but is correlated to the heating of the gold donor layer.

In order to explain the source of these observed emissions, the formation of an laser-induced plasma is considered. Plasma formation is expected only for vaporized gold. Here, volumetric heating across the donor layer is assumed. This is a valid assumption, as the thermal penetration depth δ

$$\delta = 2 \cdot \sqrt{\alpha \cdot \tau}\,, \qquad (1)$$

with the thermal diffusivity $\alpha=12.8\cdot10^{-5}\,m^2s^{-1}$ and the time $\tau=6$ ns, exceeds the donor layer thickness by one order of magnitude. Hence, the minimal fluence level F_{vap} to induce plasma is the fluence level that is needed to fully vaporize the donor layer. This threshold fluence can be estimated from

$$F_{vap} = d \cdot (Cp \cdot \Delta T + \rho \cdot (Lm + Lv))/(1 - R)\,, \qquad (2)$$

with the temperature difference $\Delta T=2829$ K, the density $\rho=19300\ kg\ m^{-3}$, the latent heat of melting $Lm=0.6\cdot10^5\ J\ kg^{-1}$, the latent heat of vaporization $Lv=1.6\cdot10^6\ J\ kg^{-1}$, the heat capacity $Cp=2.48\cdot10^6\ J\ m^{-3}K^{-1}$ and the reflection coefficient $R=0.64$. F_{vap} is calculated to be 1089 mJ/cm^2. In contrast, the observed radiation in figure 2 is detected at fluence levels, well below the calculated threshold of vaporization. Hence, the formation of a laser-induced plasma appears to be unlikely and is excluded to explain the observed emissions.

A second cause of the observed emissions may be found in the thermal emission (Planck emission) due to the high temperature of the heated gold layer. The emitted spectral irradiance as a function of the emission wavelength λ and the gold temperature T is described by Planck's equation :

$$I_\lambda(\lambda,T) = \frac{2\pi hc^2}{\lambda^5}\left[1/(e^{hc/(\lambda k_B T)} - 1)\right], \qquad (3)$$

with the Planck constant $h=4.14\cdot10^{-15}$ eV s, the speed of light $c=3\cdot10^8\ m\ s^{-1}$ and the Boltzmann constant $k_B=8.62\cdot10^{-5}\ eV\ K^{-1}$. Figure 6 shows the corresponding calculated spectral irradiance as a function of the emission wavelength, at three temperatures. The temperatures of 300K, 1337K and 3129 K correspond to the room-, melting and vaporization temperature of gold, respectively.

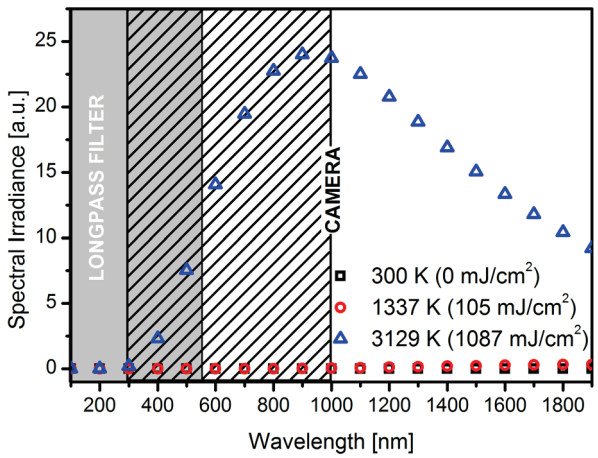

Fig. 6 Spectral irradiance calculated for three temperatures (300K, 1337K and 3129K) of gold as a function of the wavelength. The gray area indicates the spectrum blocked by the longpassfilter that was used to supress the LIFT laser pulses. The hashed area indicates the spectal sensitivity range of the camera.

The corresponding fluence values were obtained by equation 2. The range of the spectral sensitivity of the camera (about 300 nm to 1000 nm) is indicated by the hashed area in figure 6. The long-pass laser filter that was used to block the LIFT laser beam is indicated by the grey area (about 100 nm to 550 nm). As can be observed, heating of the gold above the melting temperature results in a significant increased Planck emission within the sensitive spectral range of the camera. This readily explains the observed emissions. This assumption is supported by additional analysis of side view images.

That is, figure 7 (a) shows a sketch that indicates the integration time - i.e. time period in which the shutter is open - of the camera shutters, as well as the duration of the strobe laser pulses. This scheme is key to understand the observed emissions. As indicated in fig 7 (a), the strobe pulse was triggered at the end of image A and the beginning of image B. Figures (b) and (c) show the ejection of a droplet in this time scheme. Both images indicate a bright trace of light, which is located either at the following (A image) or the leading edge (B-image) of the ejected droplet. As already discussed, it is assumed that the heated droplet constantly emits Planck radiation, which is captured by the camera as long as the shutter is open. Therefore, the observed trace of bright light is the result of the trajectory of the ejected droplet. Here, the waviness of the trace of light in figure (c), is proposed to be correlated to the ongoing deformation of the droplet during its trajectory.

4. Conclusion

An experimental study on the ejection mechanism of nanosecond LIFT was presented. Two different ejection regimes have been observed. For laser fluence values just above the transfer threshold of 140 mJ/cm^2 the formation of an liquid gold jet and the subsequent formation and ejection of single and multiple droplets are shown. Increasing fluences indicate the formation and rupture of a blistering bubble leading to an uncontrolled ejection process. Along with the ejection dynamics, the emission of a broad range source was investigated. The formation of a laser-induced

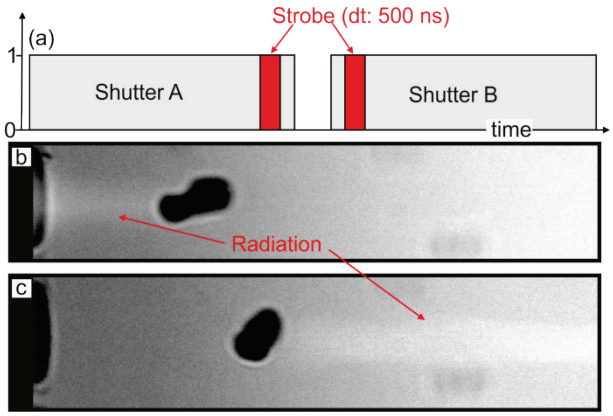

Fig. 7 (a) Sketch of the timing of the camera shutter with respect to the strobe pulses. (b)-(c) Show the donor layer on the left and the ejected droplet propagating from left to right. The ejected droplet was captured at two time instances (A- and B-images). The switching orientation of the observed bright phenomena indicates the observation of Planck radiation.

plasma was excluded and the observed emission was correlated to the thermal emission of the heated gold layer.

Acknowledgments

R. Pohl, G.R.B.E. Römer, and A.J. Huis in't Veld are grateful to the European Union Seventh Framework Programme for the funding under Grant Agreement No. 260079 (www.fab2asm.eu). C.W. Visser, C. Sun and D. Lohse acknowledge Fundamenteel Onderzoek der Materie (FOM) for funding.

References

[1] J. Bohandy, B. F. Kim and Adrian, F. J.: Journal of Applied Physics, 60, (1986) 1538 - 1539

[2] Roozeboom F., Smets M., Kniknie, B., Hoppenbrouwers, M., Dingemans, G., Keuning, W., Kessels, W., Pohl R. and Huis in 't Veld A.: 46th IMAPS International Symposium on Microelectronics (2013)

[3] D. Young, R.C.Y. Auyeung, A. Piqué, D.B. Chrisey, Dana D. Dlott: Appl. Surf. Sci., 197-198, (2002) 181-187.

[4] M. Duocastella, J.M. Fernández-Pradas, P. Serra, J.L. Morenza: Appl. Phys. A , 93, (2008) 453-456.

[5] Brown, Matthew S.; Brasz, C. Frederik; Ventikos, Yiannis et al.: J. Fluid Mechanics, 709, (2012) 341 – 370.

[6] Romain Fardel, Matthias Nagel, Frank Nüesch, Thomas Lippert andAlexander Wokaun: J. Phys. Chem. C, 114, (2010) 5617 – 5636.

[7] Y. Nakata, T. Okada, Appl. Phys. A, 69, (1999) 275-278.

[8] T. Sano, H. Yamada, T. Nakayama, I. Miyamoto, Appl. Surf. Sci., 186, (2002) 221-226.

[9] I. Zergioti, D.G. Papazoglou, A. Karaiskou, C. Fotakis, E. Gamaly, A. Rode, Appl. Surf. Sci., 208-209, (2003) 177-180.

[10] Merijn P. Giesbers, M.B. Hoppenbrouwers, E.C.P. Smits and R. Mandamparambil1: Proc. SPIE 9135, Laser Sources and Applications II, 91350Z (1 May 2014)

[11] R. Pohl, C.W. Visser, G.R.B.E. Römer, C. Sun, A.J. Huis in't Veld, D. Lohse: Proceedings of LAMP2013 - the 6th International congress on Laser Advanced Materials Processing, (2013) Niigata, Japan

[12] Arseniy I. Kuznetsov, Claudia Unger, J. K. and Chichkov B. N.: Applied Physics A, 106, (2012) 479 - 487

[13] R. Poh1, C.W. Visser, G.R.B.E. Römer, C. Sun, A.J. Huis in't Veld, D. Lohse: Proc. SPIE 8967, Laser Applications in Microelectronic and Optoelectronic Manufacturing (LAMOM) XIX, 89670X (6 March 2014)

[14] Samuel X Guo and Adela Ben-Yakar, Appl. Phys., 41, (2008) 185306.